JOURNAL OF MATERIALS SCIENCE 18 (1983) 2639–2649

The structure of boron in boron fibres

JAYANT BHARDWAJ
Carbide Tools Division, TRW Inc., Rogers, Arkansas, USA

AARON D. KRAWITZ
Department of Mechanical and Aerospace Engineering, University of Missouri, Columbia, Missouri 65211, USA

The structure of noncrystalline, chemically vapour-deposited boron fibres was investigated by computer modelling the experimentally obtained X-ray diffraction patterns. The diffraction patterns from the models were computed using the Debye scattering equation. The modelling was done utilizing the minimum nearest-neighbour distance, the density of the model, and the broadening and relative intensity of the various peaks as boundary conditions. The results suggest that the fibres consist of a continuous network of randomly oriented regions of local atomic order, about 2 nm in diameter, containing boron atoms arranged in icosahedra. Approximately half of these regions have a tetragonal structure and the remaining half a distorted rhombohedral structure. The model also indicates the presence of many partial icosahedra and loose atoms not associated with any icosahedra. The partial icosahedra and loose atoms indicated in the present model are in agreement with the relaxing sub-units which have been suggested to explain the anelastic behaviour of fibre boron and the loosely bound boron atoms which have been postulated to explain the strengthening mechanism in boron fibres during thermal treatment.

1. Introduction

Boron fibres have found application in fibre-reinforced composite materials [1]. They are produced by vapour depositing elemental boron onto a moving, resistance-heated tungsten wire substrate. A number of efforts have been made to elucidate the arrangement of atoms in the fibres [2–6]. This is desirable in order to relate structure to properties and as a possible means of production control. However, the problem is complicated because the diffraction patterns of as-produced fibres indicate an amorphous or microcrystalline state and the three basic polymorphs of boron are complex. The three well known polymorphs of pure boron utilize a common structural element, a nearly regular icosahedral grouping of twelve atoms. These polymorphs are:

1. alpha-rhombohedral boron (the unit cell, $a_0 = 0.505$ nm, $\alpha = 58.06°$, space group $R3m$, contains 12 atoms with an icosahedron at each of its lattice sites [7], with a density of 2.46 g cm^{-3});

2. tetragonal boron (the unit cell, $a_0 = 0.875$ nm, $c_0 = 0.506$ nm, space group $P4_2/nm$, contains 50 atoms distributed among four icosahedra and two individual atoms [8], with a density of 2.31 g cm^{-3});

3. beta-rhombohedral boron (the unit cell, $a_0 = 1.017$ nm, $\alpha = 65.2°$, space group $R3m$, contains 105 atoms [9, 10], with a density of 2.35 g cm^{-3}. The structure consists almost entirely of slightly deformed icosahedra arranged in a rather complicated array).

The fibres have both high tensile strength (2.07 GN m^{-2} or 3.5×10^5 psi) and Young's modulus (418 GN m^{-2} or 60.5×10^6 psi) [11, 12]. The strength of boron fibres is due in part to the fact that primary flaws are located at the surface and in the tungsten boride core where residual stresses are found to be compressive, thus inhibiting crack propagation. The longitudinal residual stress distribution [11] is compressive at the surface (− 1.38 GN m^{-2} or − 200 ksi), changing monotonically to a region of tensile stress within the boron sheath (1.03 GN m^{-2} or 150 ksi, maximum at about 25%

0022–2461/83 $03.00 + .12

of the fibre radius), then becoming compressive again near the boride core. The core itself is under a residual compressive stress of $-13.3\,GN\,m^{-2}$ (-190 ksi). Smith [13] found that after etching the fibre surface essentially all cases of fracture could be explained by crack initiation within the tungsten boride core. Behrendt [11] showed that etching increases the ultimate tensile strength of the fibre by causing a contraction which increases the residual compressive stress in the core.

Four factors are known to produce and influence the residual stress distribution [11, 14]:

1. volume expansion in the core due to boron diffusion and the formation of tungsten boride;
2. thermal expansion mismatch between the boride core and the outer boron mantle;
3. "boron elongation" during the deposition process;
4. quenching in the mercury electrode at the exit end of the reactor.

"Boron elongation" was first detected by Talley [15] and later studied by others [16–18]. It could be the predominant cause of the unfavourable residual stress distributions obtained at increased production speeds [14]. Mehalso [16] has suggested that each layer of boron is deposited with less than maximum density, incorporating many defects. With continued deposition at high temperature, the boron atoms diffuse inward, resulting in the densification and consequential volume expansion of the inner layers of the boron mantle. The driving force for this diffusion is the overall lowering of the energy of the system as boron atoms seek positions of lowest potential energy. Evidence for this model is given by the observation that greater boron elongations are obtained at lower deposition temperatures. It may be explained that boron atoms have greater mobility at higher deposition temperatures and attain lower potential energy positions with alacrity, thus lowering the concentration of defect deposition and the consequent elongation. Supporting evidence for this model has been given by DiCarlo [21], whose measurements show a radial density variation with a less than average density in the surface layers, suggesting a microvoid concentration gradient which decreases towards the core.

The opposite process of contraction has been observed by DiCarlo [19] on heating boron fibres. It was shown to be controlled by a thermally-activated mechanism, small temperature changes producing large increases in contraction, and found to occur in two distinct stages. For contractions less than 0.4% there was a slight drop in fibre density. With increasing contraction there was a marked increase in density. DiCarlo [19] has explained the observed initial contraction by suggesting that the boron atoms diffuse out of the sheath onto the fibre surface on heating, leaving microvoids within the amorphous sheath. The atoms surrounding the microvoids relax to partially fill the microvoid volume, thereby producing axial and radial contraction and a lower fibre density. The radial contractions are not observable because the extra boron atoms on the surface produce a net increase in fibre diameter. The extra atoms on the fibre end surfaces have a negligible effect on the axial contraction measurements. The net densification for contractions greater than 0.4% has been explained by the growth of the dense alpha-rhombohedral phase of boron on the fibre surface. The rapid diffusion of boron atoms has been explained by postulating the existence of two types of boron atoms: tightly bound and loosely bound. The tightly bound atoms are located in the regular structure of the 12-atom isosahedra, the structural sub-unit of all polymorphs. The loosely bound icosahedra, are located in regions of local disorder and thus are free to move rapidly through these regions.

The speculation of different types of bonded boron atoms may be related to the anelastic behaviour displayed by boron fibres. DiCarlo [12, 20, 21] has suggested that all nonelastic deformation in boron fibres can be explained by an anelastic model, as revealed by flexural stress relaxation and internal friction methods. The existence of an anelastic effect with a fairly well defined energy indicates some degree of crystallinity within the vapour-deposited fibres. The relaxation strength of the internal friction peaks was comparable to that predicted by Zener [22] for grain boundary sliding or a mechanism of similar nature. Although no grain boundaries have been observed in amorphous fibre boron [6], the sliding model may still be retained by considering the relaxation to occur between smaller sub-units in the boron structure. Additionally, it was found that high strains induced the activation of anelastic processes which were inhibited from operating at low strains by some unknown microstructural locking mechanism [21]. It was hypothesized that the relaxing entities are icosahedral in nature and the internal locks are

unknown atomic imperfections quenched in after deposition.

Icosahedra do not lend themselves to the construction of an ideal three-dimensional framework, and various degrees of compromise in the pattern of icosahedral linkage give rise to the observed proliferation of polymorphs [23]. The choice of framework is strongly influenced not only by the temperature during deposition, which imposes kinetic limitations on the process of crystal growth, but also by the boron source used and the choice of substrates upon which the crystals form [24, 25]. At temperatures below 1000° C, the alpha-rhombohedral polymorph is the only crystalline form of boron obtained; below 800° C the product is amorphous. At temperatures above 1500° C the beta-rhombohedral polymorph is formed and is the equilibrium phase at all temperatures between 0 K and the melting point. Beta-rhombohedral boron does not form at lower temperatures, possibly due to kinetic limitations. The tetragonal polymorph is found in the temperature range of 1000 to 1500° C, and should more correctly be referred to as tetragonal I, since at least five other polymorphs [23] lay claim to recognition in this temperature range. It is highly improbable that so many polymorphs are thermodynamically stable in this temperature range and the choice of framework appears to be kinetically determined.

Diffraction patterns obtained from fibre boron show broadened peaks and a large amount of structure relative to patterns from glassy amorphous materials; see Fig. 1a. While the broad peaks are amorphous in nature, the large amount of structure present indicates some degree of crystallinity. A radial distribution frunction (RDF) analysis by Badzian [4] of bulk amorphous boron indicated icosahedral distances between boron atoms. Katada [5] also obtained icosahedral distances from the RDF of thin films of vacuum-

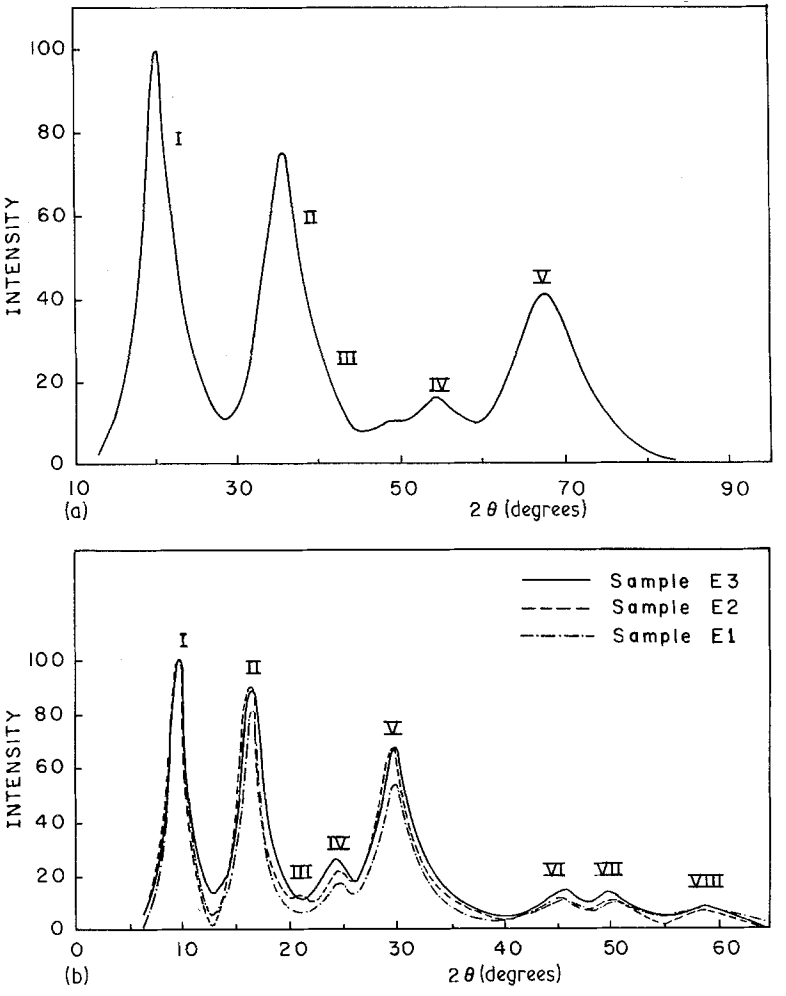

Figure 1 Debye–Scherrer patterns from (a) sample E1 (copper radiation) and (b) samples E1, E2 and E3 (molybdenum radiation). The peaks are indicated by the Roman numerals.

deposited boron. It seems natural, therefore, to assume some form of icosahedral distribution in the fibre boron structure. In addition, an attempt to explain the patterns as due to face-centred cubic arrangements of icosahedra which are heavily faulted [2] was not successful [3].

The structure of amorphous boron fibres was studied by Lindquist *et al.* [6], using X-ray diffraction and electron microscopy. Positional correlation with peaks for crystalline alpha-rhombohedral and tetragonal boron was noted, although serious discrepancies in intensity were found. This correlation led Lindquist *et al.* [6] to suggest a microcrystalline structure with an average crystallite size of about 3 nm based on peak breadth. The discrepancies in intensity were qualitatively attributed to a defect structure closely related to the alpha-rhombohedral and tetragonal structures and involving misplaced single boron atoms.

Comparisons between theoretical models and experimental results have been predominantly based on the RDF. It is of interest, in appropriate cases, to compare the calculated diffracted pattern directly with the experimental pattern. It was decided to use this approach in the present study to investigate the structure of fibre boron.

The research was begun by investigating the possibility that the structure of boron fibres was microcrystalline in nature and based on one or more of the three polymorphs of boron, as suggested by Lindquist *et al.* [6]. The Debye scattering equation [26] was used to calculate the diffracted intensity from a microcrystalline material. The coordinates of distributions of up to 1400 boron atoms were used to compute theoretical diffraction patterns. The atom positions were then changed, i.e. distortions were introduced, as well as the size and shape of the regions, until the calculated diffraction pattern bore a fair resemblance to the experimentally obtained diffraction pattern. The following sections explain the methods utilized to record the experimental diffraction patterns, model the structural ordering, and compute diffraction patterns for amorphous fibre boron.

2. Experimental procedures

2.1. Fibre production/sample preparation

The 203 μm (8 mil) diameter boron fibres used in this investigation were supplied by Avco through NASA. During production the tungsten wire substrate reacts to produce a W_2B_5 inner core and a WB_4 outer core. There is a well defined interface between the tungsten boride core and the surrounding sheath, which consists of essentially pure (99.9%) boron. The fibres were prepared as hollow cylinders, i.e. the tungsten boride core was removed, because the overwhelming X-ray scattering of tungsten relative to boron made quantitative analysis impossible. Three samples were produced, E1, E2 and E3, with outer diameters of 159 μm (6.3 mil), 182 μm (7.2 mil), and 177.6 μm (7.0 mil), and inner diameters of 45 μm (2 mil), 20 μm (0.8 mil), respectively. Etching procedures can be found in [27].

2.2. X-ray and densitometer procedures

A Debye–Scherrer camera equipped with vacuum and Gandolfi rotation [28] capability was used with an incident beam graphite crystal monochromator. The camera chamber was evacuated to less than 10^{-3} mm of mercury to reduce air scattering. The X-ray generator was operated at 45 kV and 15 mA with exposure times of 21 and 60 h, respectively, for copper and molybdenum patterns. A densitometer was used to convert the film patterns to relative intensity units. The photographic density was not allowed to exceed an experimentally determined linear response limit [27, 29] established by a series of standard calibrating exposures [29]. The transmitted light data T_i were correlated to the X-ray intensity data I_i, by statistically fitting all of the data points to a logarithmic curve $I_i = a + b \ln (100/T_i)$. The correlation coefficients were always greater than 0.96 and the results were reproducible. Calibration runs were performed before and after each measurement in order to establish the values of a and b used to convert transmission values to intensity units. After subtracting the intensities due to the inherent background density of the film and the air scattering, the remaining intensity was attributed to scattering from amorphous boron, and was converted to relative intensity units and plotted on a scale ranging from 0 to 100. The variation utilizing this technique to obtain the final relative intensity results was experimentally established to be less than 2%.

3. Computer modelling

3.1. Calculated patterns

The Debye scattering equation [26] was used to calculate diffracted intensity distributions from the model structures. The average intensity in electron units diffracted from rigid arrays of atoms

having random orientation in space is given by:

$$I_{eu}(k) = \sum_m \sum_n f_m(k) f_n(k) \sin(kr_{mn})/kr_{mn} \quad (1)$$

where $f(k)$ is the atomic scattering factor for a boron atom, k is $(4\pi \sin\theta)/\lambda$, θ is the angle of diffraction, λ is the X-ray wavelength, and r_{mn} is the interatomic distance between the atoms m and n of the rigid array. The Debye equation computes, in effect, the intensity diffracted by a matrix consisting of randomly oriented microcrystallites of the same rigid array of atoms.

A computer program was written to generate the coordinates of all the atoms in a microcrystal from one lattice point then calculate the coherent scattering per microcrystal in electron units, $I_{coh}(k)$. $I_{coh}(k)$ was corrected for polarization, $P(k)$, after which the Compton modified intensity [30] (corrected for the Breit–Dirac recoil factor) was added. The net scattered intensity was then corrected for absorption, $A(k)$. The final intensity is given by:

$$I_{eu}(k)/N = (I_{coh}(k) \times P(k)/N + I_{incoh}(k)/N) \times A(k) \quad (2)$$

where N is the number of microcrystals in the diffracting volume. Finally, the total scattered intensity was scaled so that the most intense peak was equal to 100 units, thus facilitating comparison between experimental and the computed patterns. Full details may be found in [27].

3.2. Distortion and fitting procedures

Initial models were constructed by taking unit cells of the polymorphs of boron and stacking them together in a brick-like fashion to produce an array of atoms. These arrays are identical to those found in crystalline boron, the size of the array being limited by the extent of the experimental broadening observed. Larger arrays produce sharper peaks with more peak resolution.

These initial models compared poorly with the experimentally obtained patterns. Since the fibre is produced in a metastable state, it seemed reasonable to consider the possibility that the atoms do not sit on ideal crystallographic sites. In the alpha-rhombohedral microcrystal, various triclinic distortions were introduced into the rhombohedral cell; the icosohedra were distorted by suitable random perturbations; and, microcrystals of different shapes were generated.

An interatomic distance analysis program was written which calculated the various r_{mn} terms, bracketed to within 0.001 nm, and the multiplicity of their occurrence [27]. This enabled a plot of multiplicity, M, against r_{mn} to be generated, in effect an RDF for the microcrystal. It then calculated $M(\sin kr_{mn})/kr_{mn}$ against r_{mn} for a specified k. Thus the contribution of any interatomic distance to any portion of the diffraction pattern could be discerned. This procedure was valuable in choosing distortions which eliminated unfavourable interatomic distances.

4. Results and discussion

4.1. Experimental patterns

The diffracted intensity profile obtained using copper radiation and sample E1 is shown in Fig. 1a. The absence of a peak at $2\theta = 43°$ in amorphous boron is the first noticeable discrepancy with the peak intensities of alpha-rhombohedral or tetragonal boron. In addition, the experimentally observed peak at $2\theta = 54°$ for amorphous fibre boron is very weak in both crystalline polymorphs, further indicating the inadequacy of simple microcrystalline models.

The initial part of the modelling and fitting was done using copper radiation. To insure a good fit at larger k values, molybdenum radiation was used; the diffracted intensity profiles obtained from samples E1, E2 and E3 are shown in Fig. 1b.

The patterns were independent of sample rotation, indicating that the regions of local atomic ordering are randomly oriented and small. The use of the Gandolfi attachment also produced no changes, indicating that preferred orientation (texture) effects are negligible [29].

4.2. Undistorted microcrystals of boron polymorphs

Initial diffracted intensity profiles were computed using microcrystalline models of the various boron polymorphs. Alpha-rhombohedral microcrystals were fashioned in $3 \times 3 \times 3$ (324 atoms) and $4 \times 4 \times 4$ (768 atoms) unit cell blocks; see Fig. 2a. The computed peak positions show general agreement, however, the relative intensities differ greatly. The $4 \times 4 \times 4$ model shows more structure than the $3 \times 3 \times 3$ model or the experimental pattern, and both models indicate peak III more clearly than the experimental pattern which only suggests a shoulder. The intensity ratio of peak I to peak II is much greater in the models than the

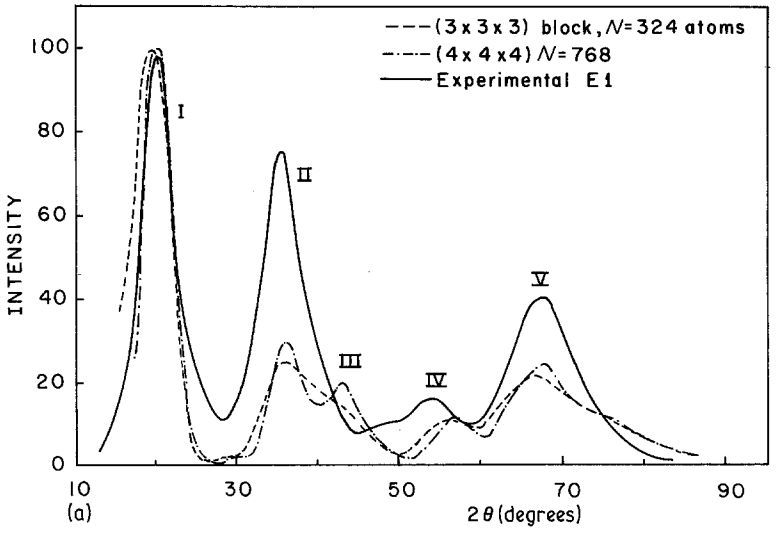

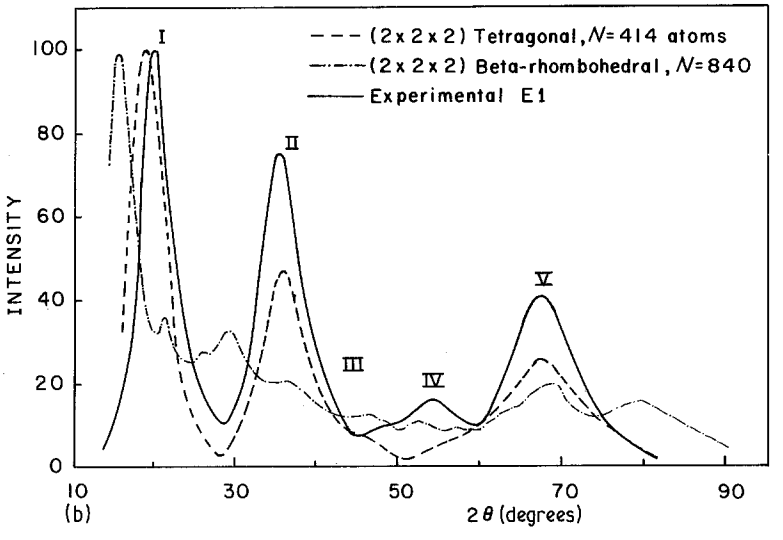

Figure 2 (a) Calculated diffraction patterns from alpha-rhombohedral microcrystals (copper radiation). (b) Calculated diffraction pattern from tetragonal and beta-rhombohedral microcrystals (copper radiation).

actual fibres. The tetragonal model is a 2 x 2 x 2 block (414 atoms); see Fig. 2b. Again the I:II ratio is higher for the model, though closer to reality than the alpha-rhombohedral models. Peak IV is not resolved though it appears in the powder pattern for the crystalline tetragonal phase [23]. The 2 x 2 x 2 model for beta-rhombohedral (840 atoms), Fig. 2b, has little in common with the experimental pattern. It was concluded that icosahedral structural units are present and that their spatial arrangement bears some relationship to that found in the alpha-rhombohedral and tetragonal polymorphs.

4.3. Distorted models

The alpha-rhombohedral structure was pursued because of the features of the 3 x 3 x 3 model, the relative simplicity of the structure, and density considerations to be discussed below. In this structure the icosahedra are not regular. Six of the boron atoms are 0.1679 nm from the centre and tend to be aligned along the rhombohedral axes, while the remaining six are 0.1695 nm from the cell centre. Based on the fitting techniques discussed in Section 3.2, r_1 to r_6 were changed from 0.1679 to 0.16 nm; r_7 to r_{12} from 0.1695 to 0.19 nm; and the cell parameter was changed from 0.5057 to 0.52 nm. The intensity obtained from a model with this applied distortion, labelled D2 (1.6, 1.9) 5.2 (see Fig. 3), showed some improvement over the undistorted model.

The application of further distortions was guided by two considerations: density and nearest-neighbour bond distance. The X-ray density of a microcrystal must be greater than or equal to the experimentally reported density [5] of fibre boron,

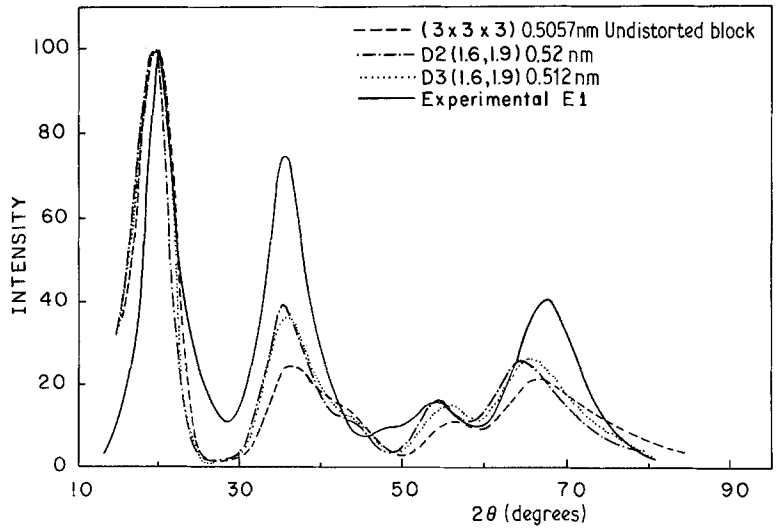

Figure 3 Calculated diffraction patterns from distorted alpha-rhombohedral microcrystalline models (copper radiation). Distortions are explained in the text. Number of atoms in models $N = 324$.

2.3466 g cm^{-3}. As no evidence of grain boundaries has been observed, a value close to the empirical value cited for the fibres is expected, implying that the matrix consists of a continuous network of randomly oriented regions possessing a characteristic average structural order. Also, the fibre density is greater than that for tetragonal and less than that for alpha-rhombohedral boron. This rules out a structure consisting purely of tetragonal boron, though a variant of alpha-rhombohedral boron or a mixture of the two polymorphs is possible. Since there are 12 boron atoms per unit cell of alpha-rhombohedral boron, the average cell parameter of a purely alpha-rhombohedral based structure must be $\leqslant 0.514$ nm. We also take the minimum nearest-neighbour distance to be 0.165 nm. This is the smallest reported nearest-neighbour spacing in any of the polymorphs of crystalline boron.

Based on the above constraints, further distortions were attempted [27]. The most successful of these was D3(1.6, 1.9)5.12, where r_1 to r_6 are 0.16 nm, r_7 to r_{12} are 0.19 nm and the cell parameter is 0.512 nm. Calculated patterns for a 3 x 3 x 3 cell model is shown in Fig. 3. An analysis of the contributions made by the various *intra*-icosahedral distances to the first and second peaks in a 3 x 3 x 3 cell array was made using the program described in Section 3.2. It was found that though the D3 distortion reduced the disparity between the first and second peaks through the applied *intra*-icosahedral distortion, other *inter*-icosahedral distances were also altered, several of which offset the improvement. Only an overall increase in the multiplicities of favourable distances would improve the fit.

One way to enhance favourable distances, and

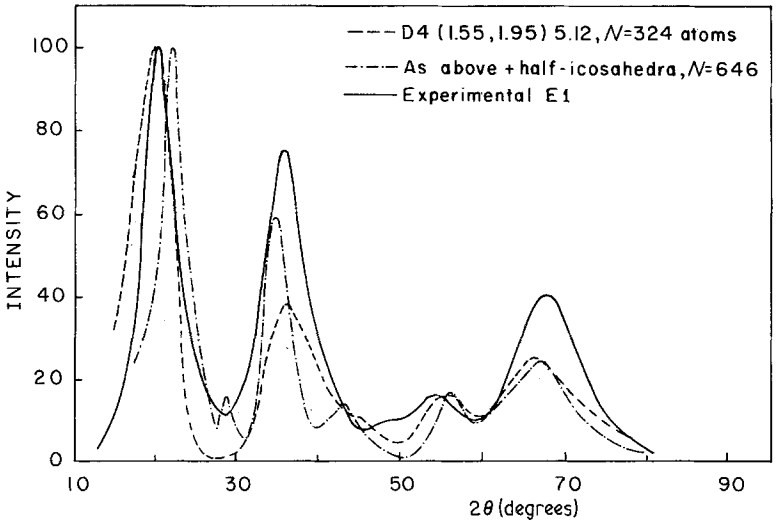

Figure 4 Calculated diffraction pattern from distorted alpha-rhombohedral microcrystals with half-icosahedra added at the periphery (copper radiation).

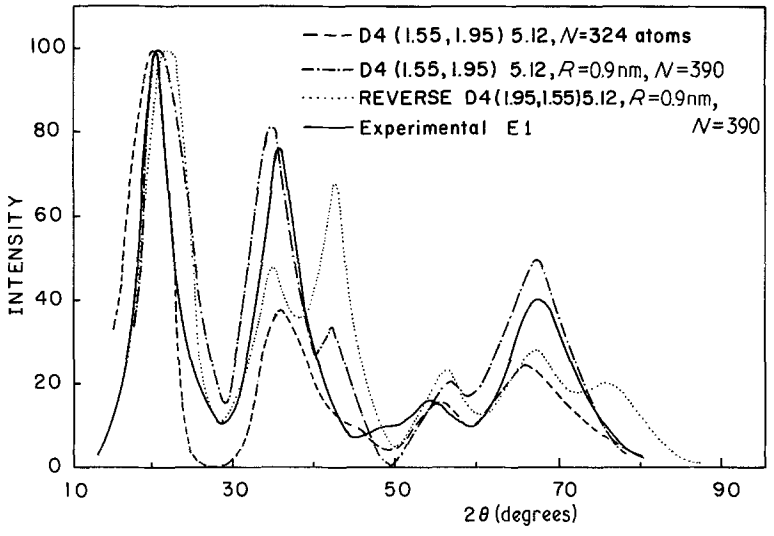

Figure 5 Calculated diffraction patterns from a spherical array of distorted alpha-rhombohedral microcrystals with partial icosahedra. A "reversed" distortion is included to show the sensitivity of the modelling process to distortions (copper radiation).

to provide a means for the contiguous connection of microcrystalline regions, is the inclusion of partial icosahedra at the surface of a microcrystal. This was done initially by adding half-icosahedra to a 3 x 3 x 3 rhombohedral block. In addition, a modified icosahedral distortion was employed, D4(1.55, 1.95)5.12. Results with and without the extra half-icosahedra are shown in Fig. 4. Further refinement was achieved by generalizing to a variety of partial icosahedra through the introduction of a spherical microcrystal which could be constructed from an array of icosahedra using the centre of an icosahedron as the origin. The surface of the sphere will intersect some icosahedra, thus producing incomplete peripheral icosahedra. The size of the microcrystal and the ratio of complete-to-incomplete icosahedra are functions of the radius R of the microcrystal. The diffraction pattern computed using icosahedra with the D4 distortion and a spherical microcrystal of radius 0.9 nm, containing 390 atoms, is displayed in Fig. 5. Some insight into the uniqueness of this model can be gained through examination of a "reverse D4" distortion, for which r_1 to r_6 are changed from 0.155 to 0.195 nm and r_7 to r_{12} are changed from 0.195 to 0.155 nm for the same spherical microcrystal. The result of this is shown in Fig. 5 where it is clear that peaks II and III have been strongly altered and a new peak at $2\theta = 78°$ has appeared. Other distortions confirmed that the ratio of intensities of peaks II and III is a sensitive function of the nearest-neighbour distances within an icosahedron.

A final distortion was settled upon, D6(1.5, 2.0)5.12. Spherical microcrystals of the D6(1.5, 2.0)5.12 distortion with radii of 0.9, 1.0, and 1.3 nm were used to compute the diffraction patterns in Fig. 6a. The $R = 1.0$ nm model displayed the best fit with the experimental pattern and had the highest second-to-third peak ratio. In order to insure that the fit was good to larger k values, the computed profile for the D6(1.5, 2.0)5.12 model was compared with the experimental profile obtained using molybdenum radiation; see Fig. 6b. It was not possible to carry this distortion technique further since some atoms would develop nearest-neighbour distances smaller than 0.165 nm, the smallest interatomic distance found in the naturally occurring polymorphs of boron. Improvements were required to fit the minor peaks, and all attempts to shift the third peak into the second peak were unsuccessful. This led to the consideration of spherical microcrystals of tetragonal boron.

The pattern computed from spherical microcrystals of tetragonal boron is displayed in Fig. 7. The first peak is broad, reflecting the two major crystalline peaks that occur in the vicinity of the first experimental peak. Attempts to shift peaks VI and VIII with the use of distortions were unsuccessful. Comparing the tetragonal and the distorted alpha-rhombohedral spherical microcrystals, it is seen that the alpha-rhombohedral model has an unwanted third peak while the tetragonal model has a shoulder. On the other hand, the alpha-rhombohedral model fits the fourth peak well while the tetragonal model has only a shoulder. This suggested the possibility that while the sample may be composed of randomly oriented small regions of structural order, some regions

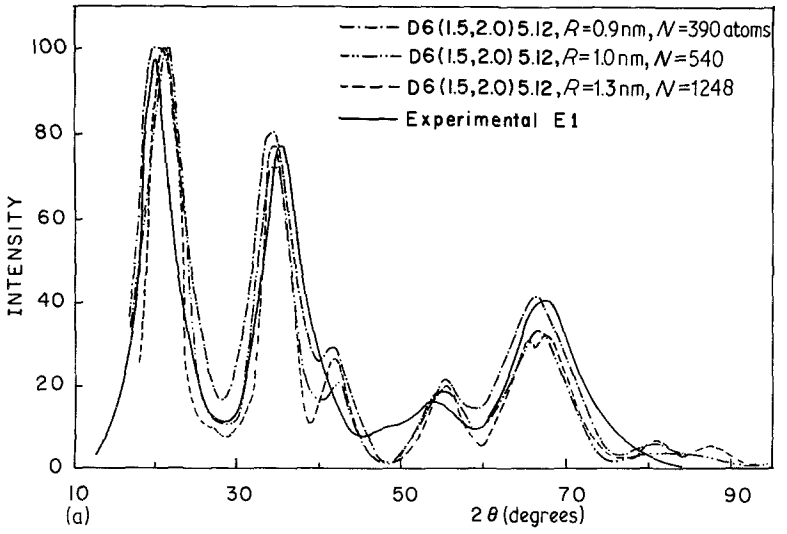

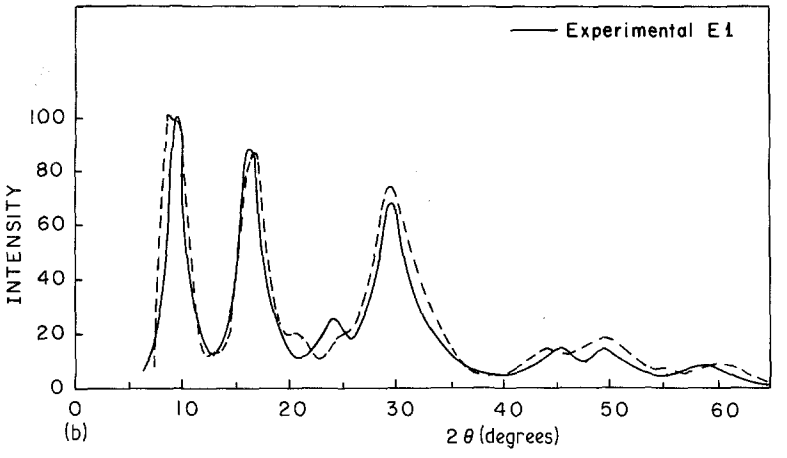

Figure 6 (a) Calculated diffraction pattern of spherical alpha-rhombohedral microcrystals showing the effect of microcrystal size (copper radiation). (b) Calculated diffraction pattern from spherical alpha-rhombohedral microcrystals with D6(1.5, 2.0)5.12 distortion and 10 nm radius (molybdenum radiation).

may have rhombohedral and others tetragonal order. This is physically reasonable since boron fibres are produced in a temperature range intermediate to those required for the production of crystalline alpha-rhombohedral and tetragonal boron. Various mixtures of the two types of spherical microcrystals of different diameter were tried. The best pattern was obtained from a model containing 50 vol% of each type, all microcrystals having a radius of 1.0 nm.

The completed pattern is shown in Fig. 8. The peak positions display reasonable agreement with

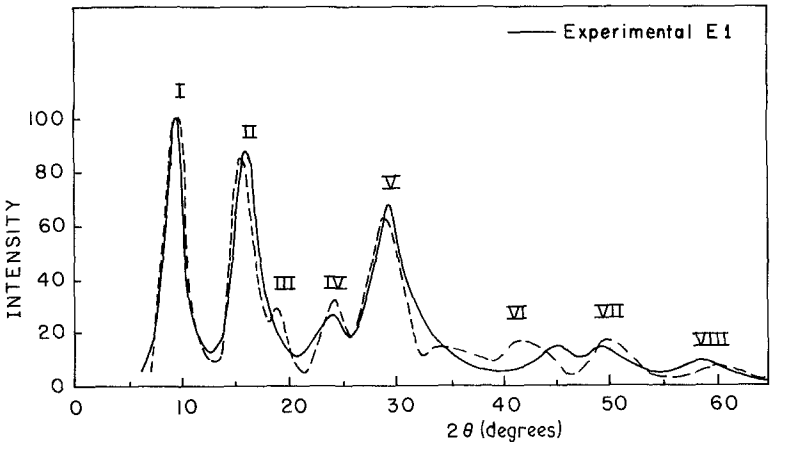

Figure 7 Calculated diffraction pattern from spherical array of tetragonal microcrystals (molybdenum radiation).

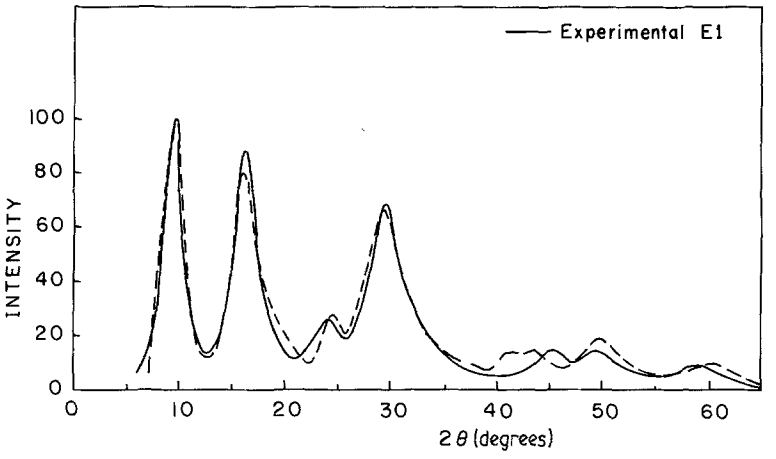

Figure 8 Final model calculated from an equal mixture by volume of the alpha-rhombohedral model shown in Fig. 6b and the tetragonal model shown in Fig. 7.

experiment, with the exception of the sixth and eighth peaks which remain somewhat displaced. The peak intensities are in good agreement. Overall this model displays the essential features of the experimentally obtained pattern. Moreover, the calculated X-ray density for this model is 2.3455 g cm^{-3}, very close to the experimental value, 2.3466 g cm^{-3}.

5. Conclusion

A model for the structure of fibre boron has been developed. The model indicates that the material consists on the average of a continuous network of randomly oriented spherical regions 2.0 nm in diameter possessing two types of local atomic order. Approximately half of these regions are based upon the alpha-rhombohedral polymorph of crystalline boron. The icosahedra in these regions are distorted so as to align themselves along the five-fold axes. The icosahedral atoms lying along the rhombohedral axes tend to position themselves closer to the centre of the icosahedra relative to the other atoms. Out of 540 atoms, 276 are in 23 complete icosahedra. Of the remaining 264 peripheral atoms, there are two groups of 11, eighteen groups of 9, six groups of 6, four groups of 4, two groups of 2 and 24 individual atoms. These incomplete icosahedra provide a mechanism for the construction of a continuous three-dimensional structure that does not possess grain boundaries. The other half of the regions possess the structure of the tetragonal boron polymorph.

The proposed model may be related to known structure and property information concerning fibre boron. The calculated density is in agreement with that of fibre boron. The positions of diffraction maxima for the fibres bear more relation to the alpha-rhombohedral and tetragonal forms than to the beta-rhombohedral structure. This is consistent with the deposition temperature used to produce the fibres. Also, the bond lengths employed do not exceed known values for crystalline boron.

Studies of the anelasticity of the fibres [12, 20, 21] have suggested that it originates in the relaxation of structural sub-units. The results of this study suggest that fibre boron can be modelled by boron icosahedra sub-units as speculated by DiCarlo [21]. In addition DiCarlo's studies of fibre strengthening by heat treatment [19] led to the proposal of the presence of highly mobile, loosely bound boron atoms. The present model also accounts for such atoms.

The questions of uniqueness invariably arises in studies of this kind. The distinctive form of the diffraction pattern; the evidence of *intra*-icosahedral distances in radial distribution function analyses [4, 5]; the propensity for icosahedral coordination in boron compounds; and the considerable agreement between the calculated and measured patterns strongly support the presence of characteristic icosahedra in fibre boron. Furthermore, the sensitivity of the calculated patterns to icosahedral distortion as well as to model size and spatial arrangement of icosahedra all lend support to the proposed model. The use of a mixture of distorted alpha-rhombohedral plus tetragonal microcrystalline regions may be viewed as artificial. It is in fact possible that a continuous hybrid structure incorporating the qualities of both the alpha-rhombohedral and tetragonal structures is closer to reality. Efforts to construct such a hybrid have proven unsuccessful thus far but may yet prove feasible.

Acknowledgements

This work was performed at Rice University, Houston, Texas. The support of the NASA Materials Grant, Rice University, and the Department of Mechanical Engineering and Materials Science, Dr W. F. Walker, Chairman, is gratefully acknowledged. The assistance of Dr J. A. DiCarlo, NASA-Lewis, and the discussions with Professor S. C. Moss, University of Houston, were invaluable to this study. Mr J. A. Ehlert contributed greatly to the experimental parts of the work.

References

1. R. M. JONES, "Mechanics of Composite Materials" (Script Book Company, Washington, DC, 1975) p. 15.
2. H. A. LIPSITT and H. M. OTTE, *Phys. Status Solidi.* **13** (1966) 439.
3. P. F. LINDQUIST, M. L. HAMMOND and R. H. BRAGG, *Phys. Status Solidi* **17** (1966) K25.
4. A. R. BADZIAN, *Mater. Res. Bull.* **2** (1967) 987.
5. K. KATADA, *Jpn. J. Appl. Phys.* **5** (1966) 582.
6. P. F. LINDQUIST, M. L. HAMMOND and R. H. BRAGG, *J. Appl. Phys.* **39** (1978) 5152.
7. B. F. DECKER and J. S. KASPER, *Acta Crystallogr.* **12** (1959) 593.
8. J. L. HOARD, R. E. HUGHES, C. H. L. KENNARD, B. B. SULLENGER, H. A. WEAKLIEM, D. E. SANDS and J. L. HOARD, *J. Amer. Chem. Soc.* 85 (1963) 361.
9. R. E. HUGHES, C. H. L. KENNARD, B. B. SULLENGER, H. A. WEAKLIEM, D. E. SANDS and J. L. HOARD, *ibid.* 85 (1963) 361.
10. D. GEIST, R. KLOSS and H. FOLLNER, *Elect. Technol. Q.* **3** (1970) 109.
11. D. R. DEHRENDT, NASA Technical Report, AFML-TM-66-187 (1967).
12. J. A. DiCARLO, NASA Technical Memorandum, NASA-TM X-13882 (1978).
13. R. J. SMITH, NASA TN-D-8219 (1976).
14. B. E. WAWNER, Office of Naval Research, "Technical Report No. 1," Contract No. N00014-76-C-0694.
15. C. TALLEY, *J. Appl. Phy.s* **30** (1959) 114.
16. R. MEHALSO, PhD thesis, Rensselaer Polytechnic Institute (1973).
17. H. DEBOLT, R. DIEFENDORF, P. GRUBER, L. JOO, V. KRUKONIS, J. MCKEE and R. MEHALSO, AFML-TR-70-287 (1971).
18. R. DIEFENDORF and R. MEHALSO, "Vapor Deposition of High Strength-High Modulus Boron on a Mono-Filament Substrate",3rd International Conference on Chemical Vapor Deposition, Salt Lake City, Utah, April 1972, p. 552.
19. J. A. DiCARLO, NASA Technical Memorandum 79077 (1979).
20. *Idem*, NASA Technical Memorandum NASA-RM X-71710 (1975).
21. *Idem*, NASA Technical Memorandum NASA-TM X-72907 (1976).
22. C. ZENER, *Phys. Rev.* **60** (1941) 906.
23. J. L. HOARD and A. E. NEWKIRK, *J. Amer. Chem. Soc.* **82** (1960).
24. D. R. STERN and L. LYNDS, *J. Electrochem. Soc.* **105** (1958) 676.
25. J. L. HOARD, "From Boron to Boranes" (American Chemical Society, Washington, 1960).
26. B. E. WARREN, "X-ray Diffraction" (Addison-Wesley Publishing Company, Reading, Massachusetts, 1969) p. 117.
27. J. BHARDWAJ, PhD thesis, Rice University (1979).
28. G. GANDOLFI, *Miner. Petrogr. Acta* **13** (1969) 67.
29. H. P. KLUG and L. E. ALEXANDER, "X-ray Diffraction Procedures" (John Wiley and Sons, New York, 1974) p. 472.
30. C. H. MacGILLAVRY and G. D. RIECK (eds), "International Tables for X-ray Crystallography" Vol. 3 (Kynoch Press, Birmingham, England, 1968) p. 250.

Received 17 May 1982
and accepted 17 January 1983